Computers in Biology and Medicine 158 (2023) 106857

Contents lists available at ScienceDirect

Computers in Biology and Medicine

journal homepage: www.elsevier.com/locate/compbiomed

ETSNet: A deep neural network for EEG-based temporal–spatial pattern recognition in psychiatric disorder and emotional distress classification

Syed Jawad H. Shah [a,*], Ahmed Albishri [a,b], Seung Suk Kang [c,*], Yugyung Lee [a], Scott R. Sponheim [d,e,f], Miseon Shim [g]

[a] Computer Science, School of Science and Engineering, Division of Computing, University of Missouri-Kansas City, MO, 64110, USA
[b] College of Computing and Informatics, Saudi Electronic University, Riyadh, 13316, Saudi Arabia
[c] Department of Biomedical Sciences, University of Missouri-Kansas City, Kansas City, MO, 64108, USA
[d] Veterans Affairs Health Care System, Minneapolis, MN, 55417, USA
[e] Department of Psychiatry, University of Minnesota, Minneapolis, MN, 55455, USA
[f] Department of Psychology, University of Minnesota, Minneapolis, MN, 55454, USA
[g] Department of Electronics and Information Engineering, Korea University, Sejong-si, Republic of Korea

ARTICLE INFO

Keywords:
Deep learning
Multi-class classification
Convolutional neural networks
Region of interest
Schizophrenia, biological relatives, and healthy controls
Brain source signals
Spatiotemporal features
Psychiatric disorders
Emotional distress

ABSTRACT

The use of EEG for evaluating and diagnosing neurological abnormalities related to psychiatric diseases and identifying human emotions has been improved by deep learning advancements. This research aims to categorize individuals with schizophrenia (SZ), their biological relatives (REL), and healthy controls (HC) using resting EEG brain source signal data defined by regions of interest (ROIs). The proposed solution is a deep neural network for the cortical source signals of the ROIs, incorporating a Squeeze-and-Excitation Block and multiple CNNs designed for eyes-open and closed resting states. The model, called EEG Temporal Spatial Network (ETSNet), has two variants: ETSNet^{s} and ETSNet^{f}. Two evaluations were conducted to show the effectiveness of the proposed model. The average accuracy for the classification of SZ, REL, and HC using EEG resting data was 99.57% (ETSNet^{f}), and the average accuracy for the classification of eyes-open (EO) and eyes-closed (EC) resting states was 93.15% (ETSNet^{s}). An ablation study was also conducted using two public datasets for intellectual and developmental disorders and emotional states, showing improved classification accuracy compared to advanced EEG classification algorithms when using ETSNet^{s}.

1. Introduction

The use of neurophysiological signals, such as the electroencephalogram (EEG), has been widely adopted for the study of brain dysfunction in psychiatric disorders. Machine learning techniques have also been utilized to develop EEG-based psychiatric diagnostic systems. With approximately 450 million people suffering from psychiatric disorders worldwide, including schizophrenia, bipolar disorder, and depression [1], reliable risk prediction and diagnosis using EEG remains a challenge due to the complexity and high level of noise in EEG signals and the significant differences between healthy and mentally ill individuals.

Previous research on computer-aided diagnosis (CAD) systems for schizophrenia has focused on distinguishing individuals with schizophrenia (SZ) from healthy controls (HC). However, such systems can lead to misdiagnosis in individuals who share genetic characteristics and phenotypes (i.e., endophenotypes [2]) with SZ but do not have the disorder. To improve the accuracy of the CAD system, genetic susceptibility to schizophrenia must be taken into consideration. Including features that differentiate biological relatives of SZ (REL) from their probands can reduce the risk of misdiagnosis. Although REL shares genetic traits with SZ, they do not exhibit the disease-specific traits that are present in SZ and absent in HC [3]. As such, it is ideal to develop a CAD system for diagnosing SZ by using features derived from both REL and SZ and HC [4,5].

Machine learning techniques, such as support vector machine (SVM) and logistic regression, have been applied to EEG signals to diagnose schizophrenia [6–10]. However, these studies have only utilized straightforward EEG features at the scalp sensor level, which can limit the accuracy of the diagnosis due to the spatial resolution limitations of sensor-level signals. To improve the classification accuracy, brain source-level signals with high spatial and temporal resolution should be utilized, as they provide more rich and detailed data [11].

* Corresponding authors.
E-mail address: shs6g7@umsystem.edu (S.J.H. Shah).

https://doi.org/10.1016/j.compbiomed.2023.106857
Received 28 November 2022; Received in revised form 6 March 2023; Accepted 30 March 2023
Available online 31 March 2023

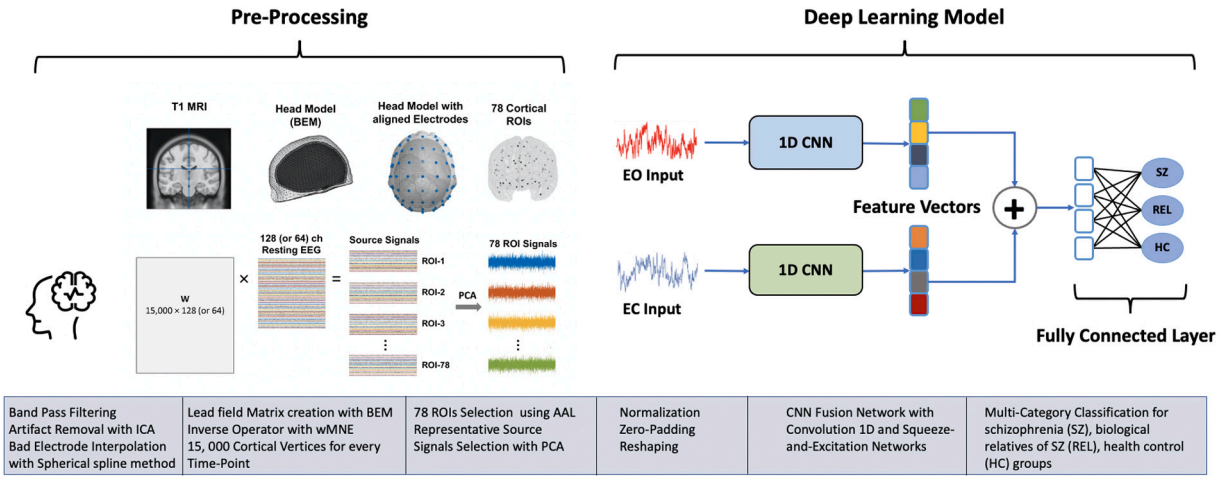

Fig. 1. End-to-end methodology diagram. The diagram illustrates the complete process from start to finish. The process begins with the collection of sensor-level EEG and MRI data from all subjects. The sensor-level signals are then processed using MRI to convert them to brain source signals. The raw brain signals undergo preprocessing before being fed into the classification model (ETSNet^{f}) for categorization.

There has been a growing interest in the use of deep learning in EEG analysis for neuropsychiatric disorders. Deep learning has the potential to provide deeper insights into EEG analysis and contribute to more effective and timely treatment of these illnesses. Recent studies utilizing deep learning models have shown significant improvements in the accuracy of classifying individuals with SZ versus HC compared to conventional machine learning methods [12–14]. Given the advancements in deep learning, it is likely that this technology will significantly enhance the CAD system for SZ diagnosis through the application of deep-learning techniques.

The aim of this work is to develop a deep learning model for the categorization of individuals with SZ, REL, and HC. The paper's contributions are summarized as follows:

- This study is the first to explore an end-to-end solution for EEG-based classification of SZ, REL, and HC to enhance the schizophrenia diagnostic classification system, as depicted in Fig. 1.
- The focus is on obtaining high spatial and temporal resolution characteristics from EEG data by computing whole-brain cortical source signals using a realistic head model built from individual magnetic resonance imaging (MRI) data.
- A novel EEG Temporal Spatial Network (ETSNet) is proposed for the cortical source signals of regions of interest (ROIs) by incorporating a Squeeze-and-Excitation block and fusing networks generated in the eyes-open (EO) and eyes-closed (EC) resting states. Two variants of ETSNet are developed: single (ETSNet^{s}), and fusion network (ETSNet^{f}).
- Extensive experiments are conducted to evaluate the performance of the proposed deep neural model in classifying SZ, REL, and HC, as well as differentiating EO vs. EC resting states. ETSNet^{f} achieved a classification accuracy of 99.57% for the 3 classes, SZ, REL, and HC. ETSNet^{s} achieved an accuracy of 93.15% in distinguishing EO vs. EC resting states.
- The performance of ETSNet^{s} is evaluated on two publicly available datasets, SEED [15] and IDD [16]. The results show improved classification accuracy on these datasets with ETSNet^{s}.

2. Related work

The primary objective of classifiers in every domain is pattern recognition. For instance, in computer vision, global and local feature recognition are used to categorize images [24] and use a variety of encryption based algorithms. In contrast to image domain, EEG data presents several challenges, including high inter- and intra-subject variance, a lack of standardization in data collection systems, and noise, which can negatively impact the classifier's ability to generalize. The type of EEG data used can also be challenging, such as in the case of creating brain computer interfaces using motor imagination data [25]. To address these cross-paradigm issues, deep neural network models, such as EEGNet [26], have been introduced to demonstrate the ability to classify EEG signals from various sources. Given the importance of EEG-based neuropsychiatric disorder diagnosis, it has received extensive research attention, resulting in the development of numerous machine learning and deep learning algorithms for handling EEG data. This section summarizes recent research on the classification of various neuropsychiatric disorders using EEG-based machine learning and deep learning techniques (as summarized in Table 1).

2.1. Machine learning for EEG classification

In the study by Alimardani et al. [17], a steady-state visual evoked potential (SSVEP) was elicited using a visual stimulus modulated at a specific frequency to perform binary categorization of bipolar and schizophrenic patients. The SSVEPs were classified based on statistical measures, including mean, skewness, and kurtosis. The study utilized five classifiers, with k-nearest neighbors (KNN) achieving the highest classification accuracy of 91.30% on resting EEG signals with a sampling rate of 250 and 21 channels from 23 patients with bipolar disorder and 23 patients with schizophrenia.

Park et al. [9] applied machine learning techniques for the classification of six major mental illnesses. They used support vector machine (SVM), Random Forest (RF), and Elastic Net Machine Learning (ENML) methods for binary classification of the six disorders, including schizophrenia, trauma/stress disorders, anxiety disorders, mood disorders, addictive disorders, and obsessive-compulsive disorder, using EEG data from 850 patients with psychiatric disorders and 95 healthy subjects. Among all these psychiatric disorders, the binary categorization between HC and SZ had the highest accuracy of 93.83%. However, their EEG data and machine learning models have not been fully validated, including for multi-class classification tasks.

2.2. Deep learning for EEG classification

Phang et al. [18] proposed a Multi-Channel Deep Convolutional Neural Network (MDC-CNN) based on parallel ensembles of 1D and 2D CNNs for classifying SZ using EEG-derived brain connectomes and investigated the integration of multiple connectivity metrics based on vector autoregressive models and partial directed coherence. They

Table 1
Comparison of studies performed on classification of various psychiatric disorders, including SZ, using EEG derived features.

Work	Data	Approach	Accuracy
Alimardani et al. [17]	EEG Resting: 23 bipolar disorder and 23 schizophrenia subjects; 250 Rate 21 Channels	SSVEP SNR features and KNN	91.30%
Park et al. 2021 [9]	EEG Resting: 19 or 64 channel from 945 subjects (850 patients with major psychiatric disorders and 95 healthy controls) binary classification of HC vs a certain psychiatric disorder	ML models: support vector machine, random forest, and elastic net	93.83%
Phang et al. 2019 [18]	EEG Resting: 45 schizophrenia patients and 39 healthy controls; 128 Rate and 16 Channels	Directed connectivity measures (VAR coefficients and PDCs) and topological CN measures MDC-CNN	91.69%
Oh et al. 2019 [12]	EEG Resting: 14 healthy subjects and 14 schizophrenia patients; 250 Rate 19 channels	CNN with 11 layers for binary classification of SZ vs. HC	98.07%
Moon et al. 2020 [19]	32-channel EEG signals from 32 subjects captured while watching 40 emotional music videos. binary classification for video emotion	CNN based on connectivity matrix that consists of Pearson correlation coefficient (PCC), phase locking value (PLV), and transfer entropy (TE). Effective data-driven approach for connectivity matrix arrangement	87.36%
Ieracitano et al. 2020 [20]	EC resting: 19 Channel EEG signals from 63 Mild Cognitive Impairment patients (MCI), 63 Alzheimer patients (AD), and 63 HC	Multi-Layer Perceptron (MLP) with Continuous Wavelet Transform (CWT) and bispectrum (BiS) features.	89.22%
RagHu et al. 2020 [21]	19-channel EEG data for 7 different kinds of seizures and 1 non-seizure	Two kinds of methodologies: 1) Transfer learning using pre-trained models, 2) Feature extraction with CNN and then classification with SVM	88.30%
Zheng et al. 2021 [13]	Two 64-channel EEG datasets. The first data is from 18 subjects that perform EO or EC while walking or standing. The second dataset is from 19 subjects placed in a virtual reality environment and completed a spatial distance monitoring task	Artificial Neural Network (ANN) or CNN with wavelet, and Hilbert-Huang Transform features.	94.93% - 99.84%
Sun et al. 2021 [14]	EEG Resting: 54 schizophrenia patients and 55 healthy controls 500 Rate; 60 Channels	FuzzyEn CNN+LSTM	99.22%
Zülfikar et al. 2022 [22]	(1) 19-channel EEG signals from 28 (14 SZ and 14 healthy controls) participants (2) 16-channel EEG signals from 84 (45 SZ and 39 healthy controls) participants	Intrinsic Mode Functions (IMF) and VGG-16 pre-trained Convolutional Neural Network (CNN) network	98.2%, 96.02%
Barros et al. 2022 [23]	schizophrenia and healthy subjects using 2D structure for each trial by stacking 1D signals captured from midline electrodes over frontal (Fz), fronto-central (FCz), central (Cz), centro-parietal (CPz), and parietal (Pz) regions of the scalp	multi-channel deep convolutional neural network for SZ and healthy control (HC) single-trial EEG	78%
Shah et al. (Ours)	EEG Resting: 21 schizophrenia patients, 20 biological relatives of the patients, 30 healthy controls; 64 or 128 channels	Independent component analysis (ICA) based Region of Interest (RoI), Fusion of 1D CNNs	99.57%

achieved an accuracy of 91.69% using resting data from 45 schizophrenia patients and 39 healthy controls, collected using a device with a sampling rate of 128 and 16 channels. Oh et al. [12] developed an 11-layer CNN model for binary classification of SZ versus HC and achieved an accuracy of 98.07% using resting data from 14 healthy subjects and 14 schizophrenia patients, collected using a device with a sampling rate of 250 and 19 channels.

Moon et al. [19] used a CNN model on the EEG-based connectivity matrix, which was composed of the Pearson correlation coefficient (PCC), phase-locking value (PLV), or transfer entropy (TE), and arranged using a practical data-driven approach. This resulted in the highest accuracy of 87.36% in emotional video classification using 32-channel EEG signals from 32 subjects captured while watching 40 emotional music videos. Ieracitano et al. [20] proposed a multi-layer perceptron that performed binary and multi-class classification using Continuous Wavelet Transform (CWT) and bispectrum (BiS) features. They evaluated the model's performance for both single and combined features and achieved an accuracy of 89.22% in multi-class classification (mild cognitive impairment (MCI) vs. Alzheimer's disease (AD) vs. healthy controls (HC)) using combined features (CWT + Bis), using 19-channel EEG signals from 63 MCI, 63 AD, and 63 HC subjects.

Raghu et al. [21] proposed two distinct classification methods for seven types of epileptic seizures using non-seizure EEG. The first method employed pre-trained CNN models and transfer learning on an EEG spectrogram, while the second technique extracted features from the spectrogram using CNN models and then classified them using SVM. They achieved an accuracy of 88.30% using the second method on 19-channel EEG signals for 7 different types of seizures and 1 non-seizure. Zheng et al. [13] introduced new measurements based on the power and frequency characteristics of wavelet and Hilbert-Huang Transform decomposed EEG signals. They used two 64-channel EEG datasets, one from 18 subjects walking or standing while performing eyes-open (EO) or eyes-closed (EC), and another from 19 subjects performing a spatial distance monitoring task in a virtual reality world. The proposed metrics were used to achieve a high classification accuracy of 94.93% to 99.84% and measurement of brain oscillations, overcoming significant variations in human scalp EEG signals.

Sun et al. [14] proposed a hybrid deep neural network by combining convolutional neural networks (CNNs) and long short-term memory (LSTM) with fuzzy entropy (FuzzyEn) and achieved an improved accuracy of 99.22% compared to an average accuracy of 96.34% using fast Fourier transform (FFT). They analyzed resting EEG data collected from 54 schizophrenia patients and 55 healthy controls using a 600-channel, 500-rate device. However, it is unclear whether the FuzzyEn model can effectively differentiate SZ from individuals with schizophrenia-like endophenotypic characteristics but did not develop the disorder.

Zülfikar et al. [22] proposed a computer-aided diagnosis (CAD) method for automatic SZ diagnosis. In this study, Hilbert Huang Transform (HHT) was used to analyze non-stationary EEG signals. The study used 19-channel EEG signals from 28 subjects (14 with SZ and 14 healthy controls) and 16-channel EEG signals from 84 subjects (45 with SZ and 39 healthy controls). The authors first generated Hilbert Spectrum (HS) images of the first four Intrinsic Mode Functions (IMF) components from the EEG data. The images were then classified using a pre-trained VGG16. By training the HS images from IMF 1 with the VGG16 pre-trained CNN, they achieved a classification accuracy of 98.2% for Dataset I and 96.02% for Dataset II.

Barros et al. [23] proposed a deep convolutional neural network to analyze EEG data from healthy and SZ individuals during passive listening. The model was trained using 5 midline electrodes (Fz, FCz,

Cz, CPz, and Pz) and was able to discriminate between SZ and HC participants with 78% accuracy. The accuracy was further improved to 80% by combining 5 fits of the model trained with varying weights. The deep network was able to automatically identify patterns in the time course and spatial distribution of EEG single-trials, detecting abnormalities in auditory processing indices in SZ patients despite its variability. The authors propose SzNet as a paradigm for future SZ research for diagnosis and prediction.

Liu et al. [27] proposed multimodal emotion recognition models using deep canonical correlation analysis (DCCA) and bimodal deep autoencoder (BDAE). They combined the models using weighted sum fusion and attention-based fusion. The study found that DCCA had a higher mean average rate on the SEED dataset [15].

These studies showcase the current advancements in machine learning and deep learning techniques for developing EEG-based automatic classification of psychiatric disorders, including schizophrenia. Table 1 summarizes previous research and compares it to our study. Our aim is to use deep learning methods to improve EEG-based multi-category (3 groups) classification, which will significantly contribute to the development of a more accurate and reliable computer-aided diagnosis system for schizophrenia.

3. Method

We present our end-to-end solution for EEG-based classification of schizophrenia (SZ), related disorders (REL), and healthy controls (HC) with the aim of improving the diagnostic classification system for schizophrenia (refer to Fig. 1). To demonstrate the efficacy of our model, we utilized three datasets: psychiatric disorders, intellectual and developmental disorder and emotional datasets. The primary dataset, which is not publicly accessible, includes EEG data from participants diagnosed with SZ, REL, and HC. The second dataset, IDD [16], includes EEG recordings from individuals with intellectual and developmental disorders. The third dataset, SEED [15], includes EEG data related to emotions from 15 subjects. The psychiatric disorder dataset and its collection, processing, and brain source computation are described in Section 3.1, while the IDD [16] and SEED datasets [15] are discussed in Section 4.1.

3.1. Psychiatric disorders dataset

3.1.1. Participants

The primary dataset in this study consisted of EEG data collected from 21 individuals diagnosed with schizophrenia (SZ), 20 with related disorders (REL), and 30 healthy controls (HC). Demographic and clinical characteristics of the participants are presented in Table 2. Recruitment of participants was carried out from various sources including hospitals, clinics, residential programs, and support programs in the Minneapolis-St. Paul metropolitan region. A doctoral-level clinical psychologist conducted structured clinical interviews using the SCID-I/P [28] and the Psychosis Module of the DIGS [29] to obtain diagnostic information for each participant. Participants who met the DSM-IV TR criteria for schizophrenia based on consensus diagnoses from multiple raters were included in the study.

The research team identified first-degree biological relatives of the patients by conducting a pedigree analysis based on the patients' reports. Interested relatives participated in a telephone interview to provide information about their demographic and medical characteristics. They were excluded from the study if they had a current or past history of psychosis or a physical condition that would prevent them from participating. Healthy control participants were recruited through advertisements at the Minneapolis Veteran Affairs Medical Center (VAMC) and in the broader urban community. The same structured clinical interview was conducted with both the related disorders group and the healthy controls group. However, only related disorders individuals without current episodes of psychopathology and only healthy controls without current or past history of psychopathology were included in the study.

Table 2
Demographic data of participants: individuals with schizophrenia (SZ), their biological relatives (REL), and healthy controls (HC).

	SZ	REL	HC
Cases #	21	20	30
Male (%)	68.2	40	54.8
Age (years)	42.4 (±9.8)	43.4 (±11.7)	46.5 (±9.1)
Edu (years)	14.8	14.8	15.2
	BPRS [30] Symptom score		
Total	44.5 (±12.6)	28.6 (±3.9)	28.9 (±4.2)
Positive	7.8 (±4.1)	3.3 (±0.7)	3.3 (±0.9)
Negative	6.3 (±3.6)	3.4 (±0.8)	3.5 (±1.3)
Disorgan.	5.5 (±2.0)	4.3 (±1.3)	3.6 (±0.8)

The severity of current schizophrenia symptoms was measured using the 24-item Brief Psychiatric Rating Scale (BPRS) [30]. Participants were excluded from the study if they met any of the following criteria: non-native English speaker, IQ of less than 70 or a diagnosis of intellectual disability, current alcohol or drug abuse, past drug dependence, current or past central nervous system disorders or conditions, medical conditions or disorders with potential central nervous system effects, history of head injury with skull fracture or loss of consciousness lasting over 20 min, and significant tardive dyskinesia as indicated by the Dyskinesia Identification System: Condensed User Scale (DISCUS) [31]. In addition, healthy control participants were excluded if they had a personal or familial history of psychotic symptoms or affective disorders.

3.1.2. EEG recordings and processes

The EEG data was collected during a resting state with a sampling rate of 1024 Hz using a 64 or 128 channel BioSemi ActiveTwo EEG device (http://www.biosemi.com/). Participants were asked to rest and close their eyes for one minute, followed by one minute of eyes-open (EO) state, and this alternated two more times (EC-EO-EC-EO) for a total recording time of four minutes. All EEG processing was carried out using Matlab software.

The EEG signals were processed as follows: first, a low-pass filter with a cut-off frequency of 128 Hz was applied, followed by down-sampling to 256 Hz using the anti-aliasing resample function. The signals were then re-referenced to the offline linked earlobe signal. A high-pass filter with a cut-off frequency of 0.5 Hz was used to reduce excessive DC offsets. Second, noisy electrode signals were identified and removed through visual inspection. Third, the EEG signals were divided into 1-second epochs for both the eyes-closed (EC) and eyes-open (EO) states. Fourth, independent component analysis (ICA) was employed to eliminate atypical noisy time segments and physiological noise such as eye movements, ECG, muscle abnormalities, electrical artifacts from the environment and electrodes. The ICA denoising process also removed poor electrode signals, which were then interpolated using the spherical spline method [32] with appropriate interpolation parameters [33]. Finally, all scalp EEG signals were re-referenced to the average signal to achieve an unbiased topographical distribution of EEG signals. For further details, refer to Kang et al. [34].

3.1.3. Brain source signal computation

T1-weighted MRI scans of all patients were acquired using an MPRAGE sequence with 240 axial slices and a slice thickness of 1 mm. These scans were used to generate individual head models from which brain source signals were computed. The surface boundaries of the gray matter, white matter, and skull were extracted using the Freesurfer tool (https://surfer.nmr.mgh.harvard.edu/). The lead field matrix that connects cortical source signals to scalp sensor data was computed using

Table 3
Data Description for the three categories: individuals with schizophrenia (SZ), their biological relatives (REL), and healthy controls (HC) before and after reshaping. The number of EEG readings increased for each category after reshaping. TL represents the fixed temporal length after zero padding, BF represents before flattening, and AF represents after flattening.

Category	#Sub	Eyes-Open (EO)			Eyes-Closed (EC)		
		TL	Shape BF	Shape AF	TL	Shape BF	Shape AF
SZ	21	57856	(21, 78, 57856)	(1638, 57856)	49152	(21, 78, 49152)	(1638, 49152)
REL	20	57856	(20, 78, 57856)	(1560, 57856)	49152	(20, 78, 49152)	(1560, 49152)
HC	30	57856	(30, 78, 57856)	(2340, 57856)	49152	(30, 78, 49152)	(2340, 49152)

the boundary element method (BEM) model, utilizing OpenMEEG and Brainstorm software [35]. The inverse operator, which converts scalp sensor signals to brain source signals, was calculated using the weighted minimum-norm (wMNE) technique from the Brainstorm toolbox [36]. The source activity of approximately 15,000 cortical vertices was computed for each time point in the temporal dimension of the source signal. 78 regions of interest (ROIs) were selected, excluding subcortical brain areas, using the Automated Anatomical Labeling (AAL) atlas [37]. The representative source signals for each of the 78 ROIs were then computed as the first principal component signal of the multiple vertex signals within each ROI, using principle component analysis (PCA). The process of generating the brain source signals using PCA is described in detail in Kang et al. [38]. The specifics of the pre-processing stage are illustrated in Fig. 1. This dataset will be referred to as the first dataset in the following sections.

3.1.4. Brain source signal preprocessing

After generating the brain source signals for the first dataset, each participant had two recordings – one for eyes-open (EO) and one for eyes-closed (EC) – with 78 regions of interest (ROIs) in each recording. The dataset consisted of EEG data from 71 participants, resulting in a total of 142 recordings. Each ROI reading was normalized using the Z-score method to facilitate comparison between variables and rescaling of other variables. The Z-score normalization was calculated using the following equation:

$$Z = \frac{x - \mu}{\sigma} \tag{1}$$

where x represents the initial feature vector, μ represents the mean, and σ represents the standard deviation. The Z-score normalization allows for standardization and enables the comparison of scores between variables.

The length of the temporal dimension for the regions of interest (ROIs) varied between subjects due to the removal of noisy time segments. To ensure uniformity in size, zero padding was applied. The longest possible temporal dimension for each activity (EO and EC) was determined, and all ROI arrays were padded with zeros to reach that fixed length. This ensured that the input data had a consistent temporal dimension. Longer classification vectors were made possible by zero padding, and zero padding in the temporal domain of the signal improves model performance [39].

After zero padding, the data had a consistent 3-dimensional shape of (S, R, T), where S represents the number of subjects, R represents the number of regions of interest (ROIs), and T represents the length of the temporal dimension. To reduce the dimensionality and augment the data, the data for each resting state was flattened by multiplying the number of subjects and ROIs. The final shape of the data was ($S \times R$, T). The reshaped data effectively increased the number of EEG readings by treating each ROI as a separate EEG recording. For example, after reshaping, the number of EEG readings for the eyes-open (EO) activity in the schizophrenia (SZ) group increased from 21 to 1638, as shown in Table 3.

3.2. Deep learning modeling

The proposed deep learning method aims to classify the brain source signals into three groups (SZ, REL, and HC) and two states (EO and EC) by utilizing feature vectors. A 1D Convolutional Neural Network (CNN) was designed for this classification task, as it is efficient with time-series data (signals) and requires fewer trainable parameters. This one-dimensional design was selected specifically for this purpose. The method consists of two different model architectures: a single CNN model (ETSNet^s) and a fusion model (ETSNet^f). These models are designed to extract and learn from data attributes automatically to improve the accuracy of the classification process.

3.2.1. Single CNN model (ETSNet^s)

The ETSNet^s architecture consists of six blocks, each consisting of a Conv1D layer, batch normalization, activation with an Exponential Linear Unit (ELU), average pooling 1D layer, dropout, and squeeze and excitation (SE) block. The final block includes Conv1D, batch normalization, ELU activation, dropout, a flattening layer, a fully connected layer, and softmax activation. The structure of the ETSNet^s is illustrated in Fig. 2.

The purpose of the Conv1D layers is to extract relevant features from the input data. These layers use filters, also known as kernels, to identify the important characteristics that contribute to the prediction. The Conv1D layer is signal-efficient as its kernel operates along a single dimension, sliding along the input signal. The dot product of the overlapping values between the kernel and the signal is calculated and the results are summed up for each kernel location during the sliding process.

parametersFor an input vector (V) of length (l) to a Conv1D layer with a kernel size (s), the convolution (V*K) can be calculated using Eq. (2). In our model, the first Conv1D layer employs 128 kernels with a size of 128, and the number of kernels and kernel size were halved in each subsequent block until the fifth block, which contains eight kernels with a size of 8. To reduce the complexity of the model, a single kernel of size 1 was used in the final Conv1D layer, as shown in Table 4.

$$(V * K)(i) = \sum_{n=1}^{s} K(n).V(i - n + \frac{s}{2}) \tag{2}$$

The description outlines the specifications of a deep learning classification model. The acronyms utilized in the explanation are explanied in Table 5.

To enhance the learning process, the model employs batch normalization to improve the efficiency of the network's learning. Instead of normalizing the entire dataset, this method is applied to individual layers and mini-batches. The mean (μ_{mb}) and standard deviation (σ_{mb}) are computed for each mini-batch and used to normalize the inputs by subtracting the mean and dividing by the standard deviation. The batch normalization process also involves the incorporation of model learning parameters, such as the scale coefficient and offset, into the inputs. The formula for batch normalization is provided in Eq. (3). In this formula, i represents the batch normalization input (from the mini-batch), α represents the element-wise scale parameter, μ_{mb} represents the sample mean for the mini-batch, σ_{mb} represents the sample standard

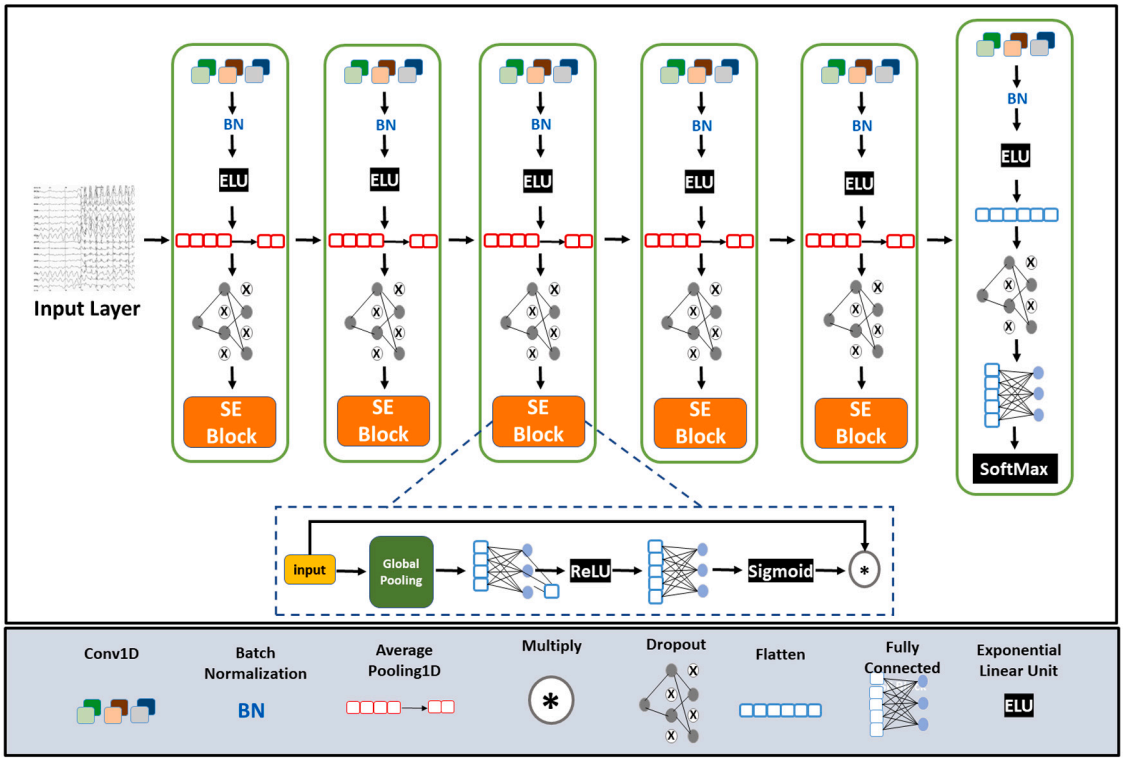

Fig. 2. The architecture of the ETSNet[s] model consists of six blocks, with the first five blocks having a similar design. Each of these blocks includes a Conv1D layer, batch normalization, activation using an Exponential Linear Unit (ELU), an average pooling 1D layer, a dropout, and a squeeze and excitation (SE) block. The final block has a slightly different design and consists of a Conv1D layer, batch normalization, ELU activation, dropout, a flattening layer, a fully connected layer, and softmax activation.

Table 4
This table provides the specifications of a deep learning classification model. The model is comprised of six blocks, each with a Conv1D layer, Batch Normalization (BN), Exponential Linear Unit (ELU) activation, and an Average Pooling layer. Each block also has a Dropout layer and a Squeeze-and-Excitation (SE) block. The final block includes a Flatten layer, Fully Connected (FC) layer, and Softmax activation function. Specific details for each block, including the number of filters (f), kernel size (k), stride (s), width (w), and ratio (for the SE block), are provided in the table. For more information on the abbreviations used, refer to Table 5.

Block	Conv1D	BN	ELU	Flatten	Average pooling	Dropout	SE block	FC	Softmax
1	f = 128 k = 128 s = 1	Yes	Yes	NA	w = 2 s = 2	0.2	ratio = 64	NA	NA
2	f = 64 k = 64 s = 1	Yes	Yes	NA	w = 2 s = 2	0.2	ratio = 32	NA	NA
3	f = 32 k = 32 s = 1	Yes	Yes	NA	w = 2 s = 2	0.2	ratio = 16	NA	NA
4	f = 16 k = 16 s = 1	Yes	Yes	NA	w = 2 s = 2	0.2	ratio = 8	NA	NA
5	f = 8 k = 8 s = 1	Yes	Yes	NA	w = 2 s = 2	0.2	ratio = 4	NA	NA
6	f = 1 k = 1 s = 1	Yes	Yes	Yes	NA	0.2	NA	n = 3 or n = 2	Yes

deviation for the mini-batch, and β represents the element-wise shift parameter.

$$BN_{mb}(i) = \alpha \odot \frac{i - \mu_{mb}}{\sigma_{mb}} + \beta \tag{3}$$

The activation function plays a critical role in the training of the model by identifying patterns in the data. It modifies the output from one layer and passes it on to the next layer as input. Our model utilized the exponential linear unit (ELU) activation function, which resulted in cost efficiencies and improved accuracy. The ELU function is depicted in Eq. (4), where x represents the input and α is a constant. For non-negative inputs, ELU behaves similarly to the rectified linear unit (ReLU) activation function, but its behavior for negative inputs differs from that of ReLU. While ReLU produces abrupt results, ELU produces smoother results.

$$E(x) = \begin{cases} x & x > 0 \\ \alpha.(e^x - 1) & x \leq 0 \end{cases} \tag{4}$$

Average pooling is employed to reduce the size of the feature map by taking the average of patches, ensuring that the compressed representation of the input signal retains all relevant information. This layer contains a condensed version of the feature maps. In our model, we used a window size of two and a stride of two for each of the five average pooling layers, as shown in Table 4. This resulted in the input being halved in size after passing through each layer.

The dropout layer was used as a regularization technique to prevent overfitting. A 20% dropout was applied in each of the model's six blocks, meaning that 20% of the neurons were randomly shut off in each of these layers to prevent overfitting. This allows the network to learn a subset of its weights in each training iteration, rather than all weights simultaneously. The output of a dropout layer, x', can be calculated using Eq. (5), where x is the input to the dropout layer and p is the probability that a neuron is dropped out.

$$x' = \begin{cases} 0 & with\ probability\ p \\ x & with\ probability\ 1 - p \end{cases} \tag{5}$$

The squeeze and excitation (SE) blocks were introduced to enhance the network's representation capabilities by adjusting the weighting of the feature maps. This was achieved by adaptively recalibrating channel-specific feature responses, and building interdependence between channels to generate feature maps [40].

The flattening layer, as its name suggests, is used to convert the feature maps into one-dimensional vectors (flattening). This layer flattens the feature maps before passing them on to the final layer of the

Table 5
Parameters for deep neural network models.

Parameter	Description
BN	Batch Normalization to improve training stability and speed up convergence by normalizing layer inputs.
ELU	Exponential Linear Unit activation, a non-linear activation function shown to improve training speed and accuracy.
SE	Squeeze-and-Excitation block, a technique that adaptively recalibrates the activations of each feature map in a CNN.
f	The number of filters (or feature maps) in a convolutional layer, which determines the dimensionality of the output space.
k	The kernel size, which determines the receptive field of a convolutional layer.
s	The stride, or the number of pixels to shift the kernel during each convolution operation. It controls the output size of a convolutional layer.
w	The window size, which determines the size of the pooling window used in a pooling layer.
FC	Fully Connected layer, a type of layer in a neural network where each neuron is connected to every neuron in the previous layer.
n	The number of neurons in a fully connected layer.

network, the fully connected (FC) layer. The FC layer's purpose is to make predictions about class labels. In our model, we used a fully connected layer consisting of either three neurons for group-based prediction or two neurons for state-based prediction, as shown in Table 4. Each neuron was connected to all data points in a one-dimensional vector generated by the flattened layer.

After the FC layer, the softmax function is applied to assign class probabilities to each input so that they sum up to 1 and each is within the range of (0,1). The mathematical formula for the softmax function is shown in Eq. (6). In this equation, S_f represents the softmax function, $\vec{x}$ represents the input vector passed to the FC layer, x_i represents all elements of the input vector to the softmax function, e^{x_i} represents the exponential function applied to each element of the input vector, and $\sum_{j=1}^{C} e^{x_j}$ represents the normalization term that ensures all probabilities given by the function will sum up to 1, with each being in the range (0,1), where C is the total number of classes (in our case, 3 for group-based and 2 for state-based prediction).

To avoid overfitting, we used an early stopping method. The Adam optimizer [41] was utilized to tune the weights and biases at each layer in the network, using a learning rate of 0.001. If the model's validation accuracy did not improve after 15 consecutive epochs of training, the learning rate was decreased by a factor of 0.1, and the validation accuracy was monitored again for another 20 epochs. If it did not improve, the training was terminated, and the test was conducted using the model with the highest validation accuracy (the maximum epochs were set to 150). The CNN model and classification process were implemented using TensorFlow. We performed hyperparameter tunning for ETSNet^s model and the results of optimal values are shown in Table 6.

$$S_f(\vec{x})_i = \frac{e^{x_i}}{\sum_{j=1}^{C} e^{x_j}} \tag{6}$$

3.2.2. Fusion model (ETSNet^f)

Additionally, we developed and evaluated a fusion model, ETSNet^f, for multi-class group-based classification based on SZ, REL, and HC. The model has two separate routes, one for Eye Open (EO) and one for Eye Close (EC). Both of these networks were developed using the corresponding data types and have a design that is similar to that of the single CNN model (ETSNet^s). The only difference was that the 1-dimensional feature vectors from both networks (EO and EC) were concatenated before being fed into the final fully connected (FC) layer and the softmax function for class prediction. This way, the model considered a feature vector containing learned features from both networks before assigning a single class label. The design of the ETSNet^f model is illustrated in Fig. 1.

The end-to-end process of our approach is summarized in Fig. 1. The raw sensor signals collected from the participants are first processed and converted into brain source signals using the participant's MRI. After minimal preprocessing, the brain source signal is fed into the model for categorization.

3.3. Model evaluation

To evaluate the performance of the proposed deep learning models, we used the K-fold cross-validation technique, which is a commonly used validation method for assessing how well a model generalizes to an independent data set. The samples were divided into 5 groups (i.e., $k = 5$), and the Leave One Out strategy was applied to each of the 5 folds to validate the model.

To measure the model's overall performance, we calculated the accuracy as the ratio of correct predictions to total predictions (Eq. (7)). Sensitivity was used to determine the model's ability to accurately identify EEG signals, defined as the fraction of actual positive cases that were predicted as positive (or true positive) (Eq. (8)). Specificity was calculated to determine the model's ability to correctly identify negative signals, defined as the fraction of actual negatives that were predicted as negative (or true negative) (Eq. (9)). Precision was used to determine the accuracy of positive predictions (Eq. (10)). The false positive rate (FPR) was used to determine the frequency of the model mistakenly recognizing background signals as EEG patterns (Eq. (11)), while the false negative rate (FNR) was used to determine the frequency of the model incorrectly identifying EEG signals as background (Eq. (12)). In the equations, TP and TN represent the number of true positive and negative cases, respectively, and FP and FN represent the number of false positive and negative cases, respectively.

$$Accuracy = \frac{TP + TN}{TP + FP + TN + FN} \tag{7}$$

$$Sensitivity = \frac{TP}{TP + FN} = 1 - FNR \tag{8}$$

$$Specificity = \frac{TN}{TN + FP} = 1 - FPR \tag{9}$$

$$Precision = \frac{TP}{TP + FP} \tag{10}$$

$$FPR = \frac{FP}{FP + TN} = 1 - TNR \tag{11}$$

$$FNR = \frac{FN}{FN + TP} = 1 - TPR \tag{12}$$

4. Results

4.1. IDD and SEED datasets

As previously noted, the experiments utilizing the IDD and SEED datasets serve to demonstrate the effectiveness of the proposed neural network model for EEG data classification, not just for psychiatric disorders. These additional datasets provide evidence that the model is suitable for classifying a variety of EEG data. The performance of ETSNet^s was evaluated against other state-of-the-art research in this field using publicly available datasets, the details of which are listed in Table 7.

The IDD dataset used in this study consisted of EEG recordings collected from 14 participants, 7 with intellectual and developmental disorders (IDD) and 7 typically developing controls (TDC), during resting-state and music stimuli [16]. The EEG data was collected using a 14-channel dry electrode EMOTIV EPOC+ device with a sampling

Table 6
Optimal hyperparameter values for the proposed CNN model.

Hyperparameter	Description	Optimal values
Learning Rate	The step size at each iteration while moving toward a minimum of a loss function. The optimal learning rate usually falls between 0.001 and 0.1.	0.001
Batch Size	The number of training examples utilized in one iteration. The optimal batch size is typically between 16 and 512.	16
#Epochs	The number of times the entire training dataset is passed forward and backward through the neural network. The optimal number of epochs can vary, but it is typically between 10 and 100 or early stopping.	150 (with early stopping)
Dropout	A regularization technique used to prevent overfitting. An optimal dropout value is typically between 0.1 and 0.5.	0.2
#Parameters (ETSNet^{f})	The total number of parameters (neurons) in the neural network that can be updated during training (Trainable) and those that remain	1.55 M/996
#Parameters (ETSNet^{s})	constant (Untrainable).	0.77 M/498
#Hidden Layers	The number of layers in the neural network that are not input or output layers. The optimal number of hidden layers may vary based on the complexity of the problem.	87 layers for ETSNet^{f} and 44 layers for ETSNet^{s}
Activation Function	introduce non-linearity in neural networks, such as ReLU, sigmoid, and tanh. ELU is a variation of ReLU that offers advantages over ReLU, such as improved performance on some datasets and reduced sensitivity to initial weights.	ELU

Table 7
EEG datasets for modeling and evaluation.

Dataset	Channel#	Subject#	Type
IDD [16]	14-channel	14 participants: IDD (7) and TDC (7)	Data → CleanData → Resting and Music
SEED [15]	62-channel	15 participants	SEED_EEG → Preprocessed_EEG

frequency of 128 Hz. For both groups of individuals, the data was presented in two formats: (1) raw EEG data and (2) pre-processed and clean EEG data [16]. In this research, the clean EEG data for resting state and music stimuli was used (Table 7), and this dataset will be referred to as the second dataset.

The SEED dataset contains EEG emotion data from 15 subjects [15]. The 62-channel ESI NeuroScan System and SMI eye-tracking glasses were used to record EEG signals and eye movements as the individuals watched four minutes of carefully selected movie snippets that were designed to evoke cohesive emotions (happy, sad, and neutral). The SEED dataset consists of two sub-datasets, SEED_EEG and SEED_Multimodal. The EEG recordings of 15 subjects are included in SEED_EEG, while SEED_Multimodal consists of EEG and eye movement data from 12 subjects [15]. For this research, only the Preprocessed_EEG data within the SEED_EEG dataset was used (Table 7), and this dataset will be referred to as the third dataset.

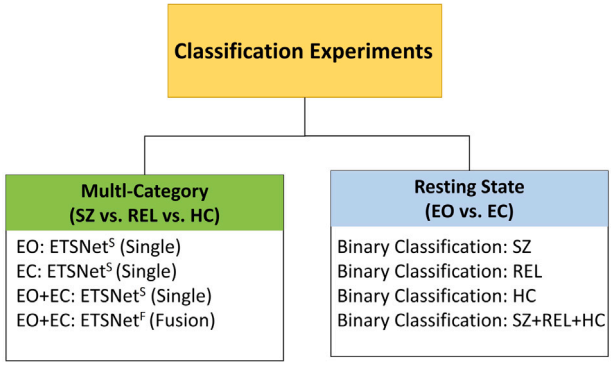

Fig. 3. The multi-class (three groups: SZ, REL, HC) and resting state (EO and EC) classification experiments with ETSNet.

4.2. Experimental design

To determine the optimal model design, the performance of 2D and 1D CNN models was compared using only the EC data. The 2D CNN model used in this comparison was similar to EEGNet [26] but included Squeeze and Excitation (SE) blocks, while the 1D CNN model was similar to the previously mentioned ETSNet^{s} but consisted of only three blocks. The accuracy of both model designs was evaluated. The 1D CNN model (ETSNet^{s}) showed better results for multi-category classification (SZ vs. REL vs. HC) on EC data with an accuracy of 91.25%, compared to the 2D CNN model which had an accuracy of 67.35%. As a result, the 1D CNN model was selected for further optimization and experimentation and was strengthened by increasing the number of blocks.

To train the proposed CNN model, it is essential to determine the optimal values of the hyperparameters shown in Table 6. These hyperparameters play a crucial role in enhancing the model's performance.

Multiple experiments were conducted on the first dataset to evaluate the performance of the ETSNet model. These tests utilized k-fold cross-validation with a value of $k = 5$. In each run, the dataset was divided into five equal parts. Four parts were used for training the model, and one part was used for testing. The values of the evaluation parameters were recorded, and this process was repeated five times to validate the model against the entire dataset. The average values for the evaluation parameters were obtained at the end. Throughout each fold, the model's best weights were saved and used to evaluate the testing data. A maximum of 150 epochs were used for training the models, with early stopping implemented to prevent the training process from continuing if the validation accuracy did not improve after 15 consecutive epochs. The results of the multi-category and binary classifications are described in Fig. 3. The results of the multi-category classification will be discussed first, followed by the results of resting state classification and a comparative evaluation.

4.3. Multi-category classifications

The multi-category classification accurately predicts the category label (SZ, REL, or HC) for an EEG signal from a specific brain source. In the first experiment, only the EO EEG signals were used to train a single CNN model (ETSNet^{s}) to classify these signals. The results of this experiment are summarized in Table 8 (a), with the model achieving an average accuracy of 96.01%, sensitivity of 95.85%, specificity of 97.92%, precision of 96.08%, false positive rate (FPR) of 2.08%, and

Table 8
ETSNet's multi-category classifications results for 5 fold cross validation.

Fold	Acc. (%)	Sens. (%)	Spec. (%)	Prec. (%)	FPR. (%)	FNR. (%)	SZAcc. (%)	RELAcc. (%)	HCAcc. (%)
(a) Classification of SZ, REL, HC Subjects using Eyes Open (EO) Data only with ETSNet^s									
1	97.20	97.08	98.51	97.45	1.49	2.92	98.47	98.56	97.38
2	95.49	95.14	97.65	95.53	2.35	4.86	97.29	96.93	96.75
3	96.48	96.35	98.19	96.46	1.81	3.65	97.74	97.83	97.38
4	95.30	95.22	97.60	95.26	2.40	4.78	97.02	97.11	96.48
5	95.57	95.46	97.65	95.69	2.34	4.54	97.83	97.11	96.21
Average	**96.01**	**95.85**	**97.92**	**96.08**	**2.08**	**4.15**	**97.67**	**97.51**	**96.84**
(b) Classification of SZ, REL, HC Subjects using Eyes Closed (EC) Data only with ETSNet^s									
1	97.20	97.11	98.54	97.32	1.46	2.89	98.29	98.47	97.65
2	97.20	97.12	98.54	97.27	1.46	2.84	98.10	98.65	97.65
3	96.48	96.54	98.21	96.45	1.79	3.45	97.74	98.19	97.02
4	97.74	97.77	98.85	97.73	1.15	2.24	98.92	98.55	98.01
5	96.84	96.98	98.41	96.65	1.59	3.02	97.83	98.55	97.29
Average	**97.09**	**97.11**	**98.51**	**97.08**	**1.49**	**2.89**	**98.18**	**98.48**	**97.52**
(c) Classification of SZ, REL, HC Subjects using Eyes Open and Eyes Closed Data (combined) with ETSNet^s									
1	93.05	93.28	96.45	92.98	3.55	6.71	96.34	96.03	93.73
2	92.23	92.10	95.99	92.30	4.01	7.90	96.03	94.85	93.59
3	91.38	91.13	95.53	91.41	4.47	8.87	94.90	94.76	93.09
4	91.78	91.45	95.70	91.99	4.30	8.55	95.40	94.81	93.36
5	90.25	90.10	95.04	90.23	4.97	9.90	93.77	94.09	92.64
Average	**91.74**	**91.61**	**95.74**	**91.78**	**4.26**	**8.39**	**95.29**	**94.91**	**93.28**
(d) Classification of SZ, REL, HC Subjects using Eyes Open and Eyes Closed Data with ETSNet^f									
1	99.37	99.41	99.68	99.36	0.32	0.59	99.64	99.73	99.37
2	99.55	99.55	99.78	99.51	0.22	0.45	99.64	99.73	99.73
3	99.64	99.57	99.80	99.69	0.20	0.43	99.73	99.82	99.73
4	99.55	99.53	99.76	99.57	0.24	0.47	99.64	99.82	99.64
5	99.73	99.75	99.86	99.72	0.14	0.25	99.82	99.91	99.73
Average	**99.57**	**99.56**	**99.78**	**99.57**	**0.22**	**0.44**	**99.69**	**99.80**	**99.64**

Multi-Class: SZ/REL/HC; SZ: schizophrenia patients; REL: biological relatives of the patients; HC: healthy controls.
Sub: Subject, Acc: Accuracy, Se: Sensitivity, Sp: Specificity, Prec: Precision, FPR: false positive rate, FNR: false negative rate, SZAcc: schizophrenic class accuracy, RELAcc: biological relative class accuracy, HCAcc: healthy control class accuracy.

false negative rate (FNR) of 4.15%. Individual class accuracies of 97.67%, 97.51%, and 96.84% were achieved for the SZ, REL, and HC groups, respectively.

In the second experiment, the performance of the EC-only CNN model was evaluated by using only EC EEG signals to train the ETSNet^s model and predict the group membership of the signals. The results of this experiment are shown in Table 8 (b). The model achieved an average accuracy of 97.09%, sensitivity of 97.11%, specificity of 98.51%, precision of 97.08%, false positive rate of 1.49%, and false negative rate of 2.89%. The average accuracy for individual classes was 98.18%, 98.48%, and 97.52% for the SZ, REL, and HC groups, respectively.

The results of the third multi-category classification experiment showed that the ETSNet^s model, when trained on both EO and EC EEG signals, had an average accuracy of 91.74%. The sensitivity was 91.61%, the specificity was 95.74%, the precision was 91.78%, the false positive rate was 4.26%, and the false negative rate was 8.39%. The individual class accuracies for the SZ, REL, and HC groups were 95.29%, 94.91%, and 93.28% respectively. These results indicate that the model performed well in predicting the group label for EEG signals from both EO and EC brain sources.

The final experiment involved using the fusion model, ETSNet^f, for multi-category classification. This model utilized both EO and EC EEG signals to predict the group label for a brain source. The ETSNet^f model consisted of two 1D CNNs, each trained on its own set of data, one for each resting state (EO and EC). The results of this experiment are summarized in Table 8 (d). The ETSNet^f model achieved an average accuracy of 99.57% with a sensitivity of 99.56%, specificity of 99.78%, precision of 99.57%, a false positive rate of 0.22%, and a false negative rate of 0.44%. The individual class accuracy for the SZ, REL, and HC groups was 99.69%, 99.80%, and 99.64%, respectively. This experiment produced the best results among all the multi-category classification experiments. Fig. 4 shows the bar graph comparison of average accuracy, sensitivity and specificity of the results shown in the Table 8. Fig. 5 shows the training and testing accuracy and loss graphs for ETSNet^f for one of the folds on 5 fold cross validation.

The results of the 5-fold cross-validation for the multi-category classification are shown in Table 9 and Fig. 6. The average results indicate that the ETSNet^f model achieved the highest accuracy on the first dataset. To better understand the relationship between the data points and classification precision, we employed t-distributed stochastic neighbor embedding (t-SNE) [42] for visualization. t-SNE is a statistical technique that maps high-dimensional data into a two-dimensional space, where each data point is assigned a location.

Fig. 7 illustrates the distances between the three categories (SZ, REL, and HC) as determined by t-SNE using resting brain source signals for EO, EC, and EO+EC. The visualization of the three classes using EC data is more distinct than that of EO, while the visualization of EO+EC has a higher number of data points and a clearer pattern than either EO or EC. This visualization highlights the relationship between the t-SNE distance and the precision of the multi-category classification on EO, EC, and EO+EC data.

4.4. Resting state classification

The resting state classification experiment aimed to predict the resting state (EO or EC) of a given brain source signal for the first dataset using only the ETSNet^s model. The experiment included four trials, each designed to classify the signal's state within a specific group (SZ, REL, HC) or across all groups (SZ+REL+HC). The results, summarized in Table 10 and depicted in Fig. 8, showed that the optimized ETSNet^s model performed well in predicting the resting state of the brain source signal, with an average accuracy of 96.25% for the SZ group, 95.29% for the REL group, 92.50% for the HC group, and 93.15% for the combined group. The model showed the highest accuracy in predicting the resting state of SZ patients.

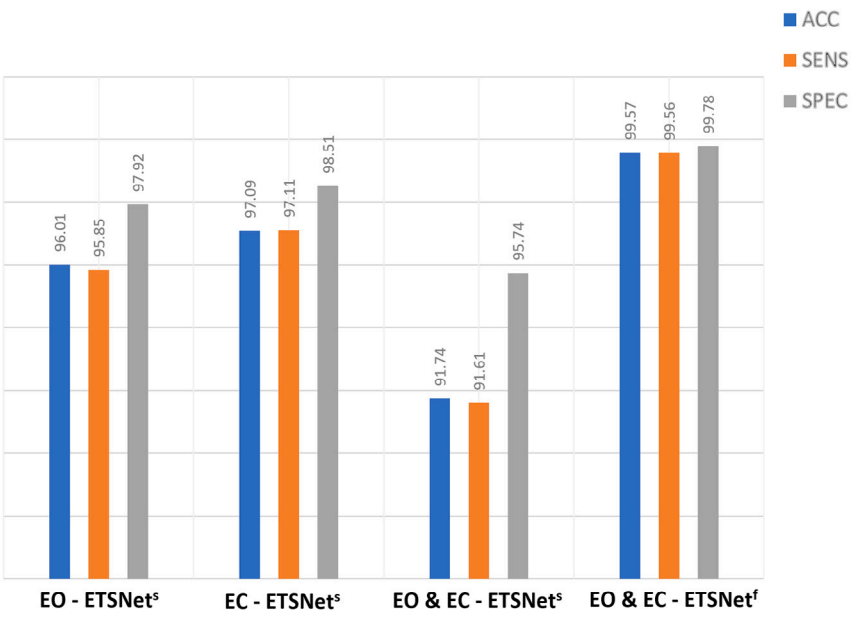

Fig. 4. The bar graph of average 5 fold accuracies (blue), sensitivity (orange) and specificity (gray) obtained for the 4 different experiments, ETSNet^s applied to EO data only, EC data only, EO+EC data, and ETSNet^f applied on EO+EC data. As seen, ETSNet^f model has achieved the best results (Table 9).

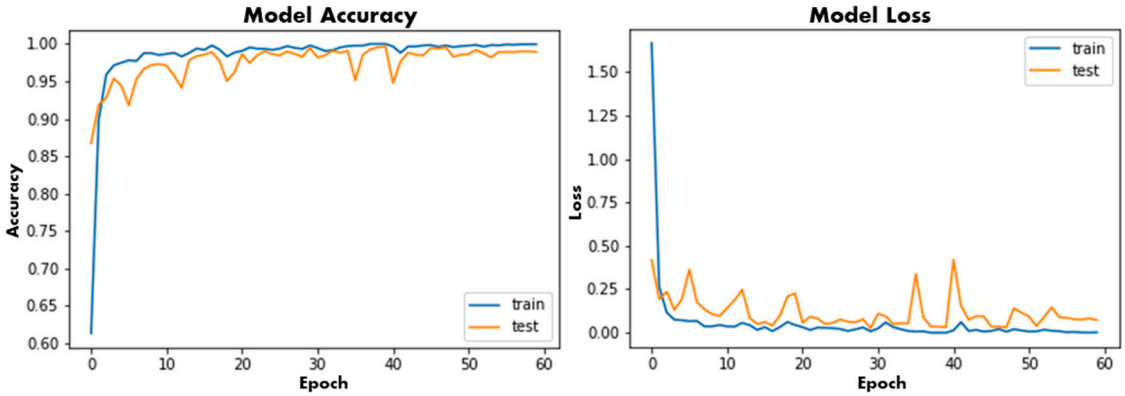

Fig. 5. Train/Test accuracy and loss graphs for ETSNet^f. The graphs are shown for only one fold of the 5 folds cross validation.

Table 9
ETSNet's Classification accuracy for schizophrenia patients (SZ), biological relatives of the patients (REL); healthy controls (HC). (Average of 5-fold cross validation).

Dataset	Multi-Class				SZ				REL				HC			
	Sub	Acc	Se	Sp	Sub	Acc	Se	Sp	Sub	Acc	Se	Sp	Sub	Acc	Se	Sp
EO	71	96.01	95.85	97.92	21	97.67	95.48	98.62	20	97.51	94.92	98.52	30	96.84	97.14	96.62
EC	71	97.09	97.11	98.51	21	98.18	97.81	98.35	20	98.48	96.55	99.25	30	97.52	96.98	97.94
EO+EC	71	91.74	91.61	95.74	21	95.29	90.36	97.36	20	94.91	91.84	96.11	30	93.28	92.64	93.75
EO⊕EC	71	**99.57**	**99.56**	**99.78**	21	**99.69**	**99.21**	**99.90**	20	**99.80**	**99.87**	**99.77**	30	**99.64**	**99.61**	**99.66**

EO: Eyes Open (ETSNet^s); EC: Eyes Closed (ETSNet^s); EO+EC: Combined (ETSNet^s); EO⊕EC: Fusion of EO & EC Models (ETSNet^f)
Sub: Subject, Acc: Accuracy, Se: Sensitivity, Sp: Specificity.

Table 10
ETSNet^s Classification Results for Eyes Open vs. Eyes Closed States for SZ, REL, HC, and SZ+REL+HC Subjects. Acc: Accuracy, Sens: Sensitivity, Spec: Specificity, Prec: Precision, FPR: false positive rate, FNR: false negative rate. Note, average results of 5 Fold Cross Validation are shown here. ETSNet^s has shown Superior performance on SZ subjects.

Class	Acc. (%)	Sens. (%)	Spec. (%)	Prec. (%)	FPR. (%)	FNR. (%)
SZ	**96.25**	**96.48**	**96.02**	**96.06**	**3.98**	**3.52**
REL	95.29	95.51	95.07	95.12	4.93	4.49
HC	92.50	90.03	94.93	94.77	5.07	9.97
SZ+REL+HC	93.15	91.42	94.85	94.76	5.15	8.58

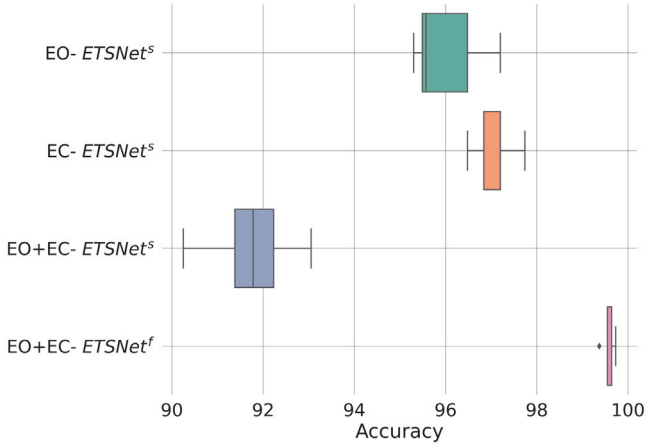

Fig. 6. The box plot of 5 fold accuracies obtained for the 4 different experiments, ETSNet^s applied to EO data only, EC data only, EO+EC data, and ETSNet^f on EO+EC data. As seen, ETSNet^f model has achieved the best results.

Table 11
Comparison of ETSNet^s and ETSNet^f with EEGNet [26] for group classification (SZ vs REL vs HC) on EO+EC data.

Method	Dimensions	Validation Accuracy (%)
EEGNet [26]	2D	82.76
ETSNet^s (ours)	1D	91.74
ETSNet^f (ours)	1D	**99.57**

4.5. Comparative evaluation with other models

For the first dataset, we compared ETSNet^s and ETSNet^f with EEGNet [26]. This model is state-of-the-art for EEG classification. The results of this comparison are shown in Table 11. The table shows that on the first dataset, ETSNet^f beat all other models, ETSNet^s came in second, and EEGNet [26] came in third. These results demonstrate the effectiveness of the proposed ETSNet^f and ETSNet^s model in EEG classification tasks.

On the EEG IDD dataset [16], the performance of ETSNet^s was compared against Quadratic Discriminant Analysis [43], Random Forest Classifier [44], and the 3D CNN model [45]. The results of this comparison are shown in Table 12. As the table indicates, two types of comparisons were made, one using cross-validation (e.g., 5-fold) and the other using a train and test split. The second dataset [16] includes two types of EEG signals: music stimuli and resting state. In this comparison, ETSNet^s achieved the best accuracy of 99.90% on the music stimuli EEG signals with a 70-30 train and test split. It also achieved the second-best accuracy of 98.47% on the resting state EEG signals using 5-fold cross-validation. The 3D CNN model [45] achieved the second-best accuracy of 99.85% on the music stimuli EEG signals and the highest accuracy of 98.87% on the resting state EEG signals with a 71-29 train and test split. Although the 3D CNN model reported slightly better results (less than a 0.5% improvement) than ETSNet^s on the resting state EEG, its architecture is more complex (3D vs. 1D for ETSNet^s) and requires additional data, and the generation of Scalograms. Furthermore, the 3D CNN model [45] was not evaluated using cross-validation, which is a more reliable indicator of model performance.

The performance of ETSNet^s on the SEED dataset [15], was compared to several other models, including SVM [46], DGCNN [47], SLFN [48], SVM and RFE [49], and DCCA [27]. The results of this comparison are shown in Table 13. Both cross-validation (f = 5) and train and test split comparisons were made. ETSNet^s achieved the highest accuracy of 98.50% when trained and tested with a split of 60 and 40, respectively. The second-best model was DCCA [27], which achieved an accuracy of 94.60% with the same train and test split. ETSNet^s also showed a comparable accuracy of 94.10% when evaluated using 5-fold cross-validation.

5. Discussion

In this study, we introduced two novel 1D CNN models, ETSNet^s and ETSNet^f, for EEG classification. The results demonstrate the effectiveness of these models in classifying psychic disorders, as well as in other EEG domains such as intellectual development disorders and emotions. Our experiments on EEG signals showed remarkable performance, which can be attributed to several factors.

- The use of 78 cortical ROI signals instead of scalp EEG signals, which provide more accurate representations of local brain signals than signals mixed from multiple regions due to volume conduction.
- The optimized design of the deep neural network that allowed the models to perform multiple classification tasks while having a minimal number of trainable parameters.
- The reshaping of the data into 1D vectors, making it suitable for a 1D CNN network, resulting in each brain source signal or channel reading being presented as a single input for predictions and increasing the size of the training and testing data.

Initially, we compared the performance of 1D CNN and 2D CNN models for EEG classification. For the EC data, we obtained an accuracy of 91.25% using the ETSNet^s model (which had only 3 blocks) and 67.35% using the 2D CNN model. To further improve the performance, we increased the depth of the ETSNet^s model, which resulted in an accuracy of 97.09% for the EC data only. The ETSNet^f model, which consisted of two separate CNN networks trained on the EO and EC data, outperformed the single ETSNet^s model trained on combined EO and EC data. The ETSNet^f model had an accuracy of 99.57%, while the ETSNet^s model had an accuracy of 91.74%. Our experiments on multiple datasets (EO, EC, EO+EC, and EO⊕EC) showed statistically significant results for multi-category classification (as shown in Table 9). Moreover, our model achieved better results compared to other state-of-the-art models on two publicly available datasets (as shown in Tables 12 and 13), demonstrating the optimal design of our model.

Interestingly, the accuracy of the EO vs. EC categorization differed between groups, with the highest accuracy being observed in the SZ group and the lowest in the HC group (refer to Table 10). The brain signals of the SZ group seemed to exhibit more pronounced differences between the EO and EC resting states. Further systematic investigations with larger sample sizes may be required to determine if the difference between EO and EC could be related to any underlying brain mechanisms specific to SZ.

The results of our multi-category classification study showed that our proposed models, ETSNet^s and ETSNet^f, outperformed the state-of-the-art binary classification models, as seen in Table 1. The improved accuracy achieved by classifying individuals into three categories (SZ, REL, and HC) is crucial for a schizophrenia CAD system, as differentiating schizophrenia from other mental disorders that have similar symptoms and genetic traits is essential. This is highlighted by Alimardani et al. [17], who used a KNN model to distinguish schizophrenia from bipolar illness.

Additionally, our results show that our proposed deep learning approach can be used to accurately distinguish between individuals with different mental health conditions, including those with schizophrenia, those at high risk of developing schizophrenia, and healthy individuals. This highlights the potential of our approach to be developed into a comprehensive CAD system for the differential diagnosis of mental disorders and the identification of individuals at risk. However, further research with larger sample sizes is needed to validate the generalizability of our findings.

Table 12
Comparison of accuracy of state-of-the-art models on the EEG IDD dataset (second dataset) [16] (cross validation and data split) with ETSNet^s. "–" indicates that the information is not reported. ETSNet^s is the best on music stimuli and second best on resting signals in this comparison.

Work	Model	Validation/Testing	Resting Accuracy (%)	Music stimuli Accuracy (%)
Anwar et al. 2020 [43]	Quadratic Discriminant Analysis	Cross Validation (7 folds)	91.90	92.60
Breitenbach et al. 2021 [44]	Random Forest Classifier	Cross Validation (10 folds)	91.67	–
Oda et al. 2021 [45]	3D CNN with Data generation	Data Split (71:29)	**98.87**	99.85
Shah et al. 2023	ETSNet^s	Data Split (70:30)	98.31	**99.90**
		Cross Validation (5 folds)	98.47	99.45

Table 13
Comparison of accuracy rates (%) of state-of-the-art models on the SEED EEG dataset [15] with ETSNet^s. The comparison was performed using a 60:40 train-test split and cross-validation with 5 folds. "–" indicates that the information is not reported. ETSNet^s achieved the best results on this dataset.

Work	Method	Validation/Testing	Class#	Accuracy (%)
Topic et al. 2021 [46]	HOLO-FM CNN+SVM	Cross Validation (10 folds)	2	88.45
Song et al. 2018 [47]	DGCNN + DE	Data Split (60:40)	3	90.40
Yang et al. 2017 [48]	SLFN	Data Split (60:40)	3	93.26
Subas et al. 2021 [49]	SVM & RFE	–	3	93.10
Liu et al. 2021 [27]	DCCA	Data Split (60:40)	3	94.60
Pusarla et al. 2022 [50]	LMD-NIG	Cross Validation (5 folds)	3	98.00
		Cross-Subject Validation	3	94.87
Shah et al. 2023 (ours)	ETSNet^s	Data Split (60:40)	3	**98.50**
		Cross Validation (5 folds)	3	94.10

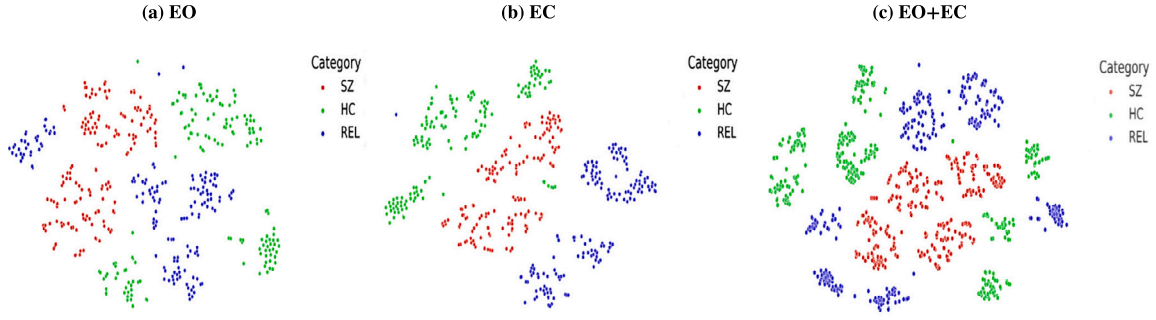

Fig. 7. This figure visualizes the distance between the three categories (SZ, REL, and HC) as represented by t-SNE in two-dimensional space, using the resting-state brain source signals for (a) EO, (b) EC, or (c) EO+EC. The visualization of the EC data shows a clearer distinction between the three categories compared to the EO visualization. The visualization of EO+EC has more data points and a clearer pattern than EO alone, but is comparable to EC. This figure highlights the relationship between the t-SNE distance and the precision of multi-category classification on EEG signals from EO, EC, and EO+EC sources.

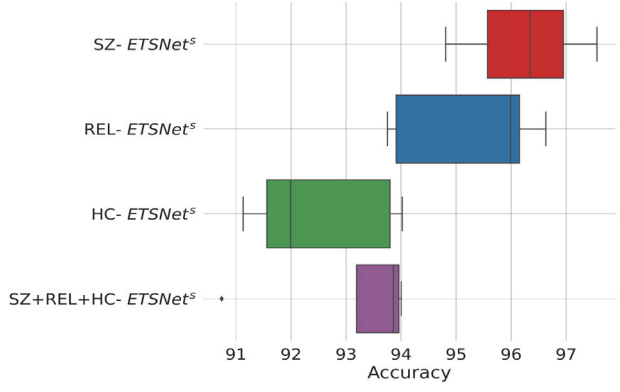

Fig. 8. The box plot displays the 5-fold cross-validation accuracies obtained in 4 different experiments of EEG data classification: EO vs EC, using the ETSNet^s model. The experiments include the application of the model to SZ data only, REL data only, HC data only, and to the combined SZ+REL+HC data. The results show that the ETSNet^s model with SZ data alone achieved the best results among the 4 experiments.

6. Conclusion and future work

This article presents a novel approach for classifying individuals with schizophrenia (SZ), relatives of individuals with schizophrenia (REL), and healthy controls (HC) using an EEG-based deep learning model. We computed the major brain source signals of 78 cortical regions of interest (ROIs) from resting EEG recordings, which were then used as input for our deep neural network. Our experiments showed that the optimized model achieved an accuracy of 99.57% for group classification and 93.15% for resting state classification (EO and EC). The high performance of the model can be attributed to its efficient architecture, which incorporated SE blocks and merged networks formed under resting state conditions, as well as the use of higher spatial resolution brain source signals compared to scalp EEG signals. Our approach represents a significant advancement in multi-category classification for SZ, REL, and HCs, with superior design and generalizability, demonstrated through comparative analysis of two publicly available datasets.

This study provides a basis for future work in the field of EEG-based schizophrenia classification. In particular, we aim to extend the current research by incorporating dynamic segmentation of EEG data with both temporal and spatial dimensions. We envision an integrated deep

learning framework that optimizes the design by seamlessly combining several deep learning models with multi-modality datasets, including Electroencephalogram (EEG), Magnetic Resonance Imaging (MRI), and Electronic Health Records (EHR). This framework will also incorporate techniques for model adaptation, such as automatic knowledge distillation and domain adaptation strategies that take into account data similarity and transfer learning. Inspired by the integrated machine learning framework proposed in [51], our goal is to create a comprehensive approach for schizophrenia categorization that leverages the strengths of multiple modalities and deep learning models.

CRediT authorship contribution statement

Syed Jawad H. Shah: Conceptualization, Methodology, Software, Writing - Original Draft, Writing - Review & Editing. **Ahmed Albishri:** Conceptualization, Methodology, Software, Writing - Original Draft, Writing - Review & Editing. **Seung Suk Kang:** Conceptualization, Methodology, Software, Data Curation, Writing - Original Draft, Writing - Review & Editing. **Yugyung Lee:** Conceptualization, Methodology, Software, Writing - Original Draft, Writing - Review & Editing. **Scott R. Sponheim:** Conceptualization, Methodology, Software, Data Curation. **Miseon Shim:** Conceptualization, Methodology, Software, Data Curation.

Declaration of competing interest

The authors declare that they have no known competing financial interests or personal relationships that could have appeared to influence the work reported in this paper.

References

[1] E.F. Augusterfer, R.F. Mollica, J. Lavelle, A review of telemental health in international and post-disaster settings, Int. Rev. Psychiatry 27 (6) (2015) 540–546.

[2] I.I. Gottesman, T.D. Gould, The endophenotype concept in psychiatry: etymology and strategic intentions, Am. J. Psychiatry 160 (4) (2003) 636–645.

[3] N.C. Venables, E.M. Bernat, S.R. Sponheim, Genetic and disorder-specific aspects of resting state EEG abnormalities in schizophrenia, Schizophrenia Bullet. 35 (4) (2009) 826–839.

[4] D.L. Braff, G.A. Light, The use of neurophysiological endophenotypes to understand the genetic basis of schizophrenia, Dialogues Clin. Neurosci. 7 (2) (2005) 125.

[5] E. Bramon, C. McDonald, R.J. Croft, S. Landau, F. Filbey, J.H. Gruzelier, P.C. Sham, S. Frangou, R.M. Murray, Is the P300 wave an endophenotype for schizophrenia? A meta-analysis and a family study, Neuroimage 27 (4) (2005) 960–968.

[6] K.S. Ambrosen, M.W. Skjerbæ k, J. Foldager, M.C. Axelsen, N. Bak, L. Arvastson, S.r.R. Christensen, L.B. Johansen, J.M. Raghava, B. Oranje, et al., A machine-learning framework for robust and reliable prediction of short-and long-term treatment response in initially antipsychotic-naïve schizophrenia patients based on multimodal neuropsychiatric data, Transl. Psychiatry 10 (1) (2020) 1–13.

[7] V. Jahmunah, S.L. Oh, V. Rajinikanth, E.J. Ciaccio, K.H. Cheong, N. Arunkumar, U.R. Acharya, Automated detection of schizophrenia using nonlinear signal processing methods, Artif. Intell. Med. 100 (2019) 101698.

[8] J.K. Johannesen, J. Bi, R. Jiang, J.G. Kenney, C.-M.A. Chen, Machine learning identification of EEG features predicting working memory performance in schizophrenia and healthy adults, Neuropsychiatric Electrophysiol. 2 (1) (2016) 1–21.

[9] S.M. Park, B. Jeong, D.Y. Oh, C.-H. Choi, H.Y. Jung, J.-Y. Lee, D. Lee, J.-S. Choi, Identification of major psychiatric disorders from resting-state electroencephalography using a machine learning approach, Front. Psychiatry (2021) 1398.

[10] W. Yassin, H. Nakatani, Y. Zhu, M. Kojima, K. Owada, H. Kuwabara, W. Gonoi, Y. Aoki, H. Takao, T. Natsubori, et al., Machine-learning classification using neuroimaging data in schizophrenia, autism, ultra-high risk and first-episode psychosis, Transl. Psychiatry 10 (1) (2020) 1–11.

[11] S.S. Kang, Addressing measurement issues in electroencephalography studies of meditations as alternative interventions of posttraumatic stress disorder, Psychol. Trauma Theory Res. Pract. Policy 12 (2) (2020) 116.

[12] S.L. Oh, J. Vicnesh, E.J. Ciaccio, R. Yuvaraj, U.R. Acharya, Deep convolutional neural network model for automated diagnosis of schizophrenia using EEG signals, Appl. Sci. 9 (14) (2019) 2870.

[13] J. Zheng, M. Liang, S. Sinha, L. Ge, W. Yu, A. Ekstrom, F. Hsieh, Time-frequency analysis of scalp EEG with Hilbert-Huang transform and deep learning, IEEE J. Biomed. Health Inf. (2021).

[14] J. Sun, R. Cao, M. Zhou, W. Hussain, B. Wang, J. Xue, J. Xiang, A hybrid deep neural network for classification of schizophrenia using EEG data, Sci. Rep. 11 (1) (2021) 1–16.

[15] W.-L. Zheng, B.-L. Lu, Investigating critical frequency bands and channels for EEG-based emotion recognition with deep neural networks, IEEE Trans. Autonom. Mental Dev. 7 (3) (2015) 162–175.

[16] E. Sareen, L. Singh, B. Varkey, K. Achary, A. Gupta, EEG dataset of individuals with intellectual and developmental disorder and healthy controls under rest and music stimuli, Data Brief 30 (2020) 105488.

[17] F. Alimardani, J.-H. Cho, R. Boostani, H.-J. Hwang, Classification of bipolar disorder and schizophrenia using steady-state visual evoked potential based features, IEEE Access 6 (2018) 40379–40388.

[18] C.-R. Phang, F. Noman, H. Hussain, C.-M. Ting, H. Ombao, A multi-domain connectome convolutional neural network for identifying schizophrenia from EEG connectivity patterns, IEEE J. Biomed. Health Inf. 24 (5) (2019) 1333–1343.

[19] S.-E. Moon, C.-J. Chen, C.-J. Hsieh, J.-L. Wang, J.-S. Lee, Emotional EEG classification using connectivity features and convolutional neural networks, Neural Netw. 132 (2020) 96–107.

[20] C. Ieracitano, N. Mammone, A. Hussain, F.C. Morabito, A novel multi-modal machine learning based approach for automatic classification of EEG recordings in dementia, Neural Netw. 123 (2020) 176–190.

[21] S. Raghu, N. Sriraam, Y. Temel, S.V. Rao, P.L. Kubben, EEG based multi-class seizure type classification using convolutional neural network and transfer learning, Neural Netw. 124 (2020) 202–212.

[22] A. Zülfikar, A. Mehmet, Empirical mode decomposition and convolutional neural network-based approach for diagnosing psychotic disorders from eeg signals, Appl. Intell. (2022) 1–13.

[23] C. Barros, B. Roach, J.M. Ford, A.P. Pinheiro, C.A. Silva, From sound perception to automatic detection of schizophrenia: an EEG-based deep learning approach, Front. Psychiatry 12 (2022) 2659.

[24] O. El Ogri, H. Karmouni, M. Sayyouri, H. Qjidaa, 3D image recognition using new set of fractional-order Legendre moments and deep neural networks, Signal Process., Image Commun. 98 (2021) 116410.

[25] S.J.H. Shah, A.A. Albishri, Y. Lee, Deep learning framework for internet of things for people with disabilities, in: 2021 IEEE International Conference on Big Data (Big Data), IEEE, 2021, pp. 3609–3614.

[26] V.J. Lawhern, A.J. Solon, N.R. Waytowich, S.M. Gordon, C.P. Hung, B.J. Lance, EEGNet: a compact convolutional neural network for EEG-based brain–computer interfaces, J. Neural Eng. 15 (5) (2018) 056013.

[27] W. Liu, J.-L. Qiu, W.-L. Zheng, B.-L. Lu, Comparing recognition performance and robustness of multimodal deep learning models for multimodal emotion recognition, IEEE Trans. Cogn. Dev. Syst. (2021).

[28] M.B. First, Structured clinical interview for DSM-IV axis I disorders, Biometrics Res. Dep. (1997).

[29] M. Preisig, B.T. Fenton, M.-L. Matthey, A. Berney, F. Ferrero, Diagnostic interview for genetic studies (DIGS): inter-rater and test-retest reliability of the french version, Eur. Arch. Psychiatry Clin. Neurosci. 249 (4) (1999) 174–179.

[30] J.E. Overall, D.R. Gorham, The brief psychiatric rating scale, Psychol. Rep. 10 (3) (1962) 799–812.

[31] R. Sprague, J. Kalachnik, D. White, Dyskinesia identification system: Condensed user scale (DISCUS), 1985, Available from the Institute for Human Research.

[32] F. Perrin, J. Pernier, O. Bertrand, J.F. Echallier, Spherical splines for scalp potential and current density mapping, Electroencephalogr. Clin. Neurophysiol. 72 (2) (1989) 184–187.

[33] S.S. Kang, T.J. Lano, S.R. Sponheim, Distortions in EEG interregional phase synchrony by spherical spline interpolation: causes and remedies, Neuropsychiatric Electrophysiol. 1 (1) (2015) 1–17.

[34] S.S. Kang, A.W. MacDonald, S.R. Sponheim, Dysfunctional neural processes underlying context processing deficits in Schizophrenia, Biol. Psychiatry Cognit. Neurosci. Neuroimaging 4 (7) (2019) 644–654.

[35] A. Gramfort, T. Papadopoulo, E. Olivi, M. Clerc, OpenMEEG: opensource software for quasistatic bioelectromagnetics, Biomed. Eng. Online 9 (1) (2010) 1–20.

[36] F. Tadel, S. Baillet, J.C. Mosher, D. Pantazis, R.M. Leahy, Brainstorm: a user-friendly application for MEG/EEG analysis, Comput. Intell. Neurosci. 2011 (2011).

[37] N. Tzourio-Mazoyer, B. Landeau, D. Papathanassiou, F. Crivello, O. Etard, N. Delcroix, B. Mazoyer, M. Joliot, Automated anatomical labeling of activations in SPM using a macroscopic anatomical parcellation of the MNI MRI single-subject brain, Neuroimage 15 (1) (2002) 273–289.

[38] S.S. Kang, A.W. MacDonald III, M.V. Chafee, C.-H. Im, E.M. Bernat, N.D. Davenport, S.R. Sponheim, Abnormal cortical neural synchrony during working memory in schizophrenia, Clin. Neurophysiol. 129 (1) (2018) 210–221.

[39] D. Gao, W. Zheng, M. Wang, L. Wang, Y. Xiao, Y. Zhang, A zero-padding frequency domain convolutional neural network for ssvep classification, Front. Hum. Neurosci. 16 (2022).

[40] J. Hu, L. Shen, G. Sun, Squeeze-and-excitation networks, in: Proceedings of the IEEE Conference on Computer Vision and Pattern Recognition, 2018, pp. 7132–7141.

[41] D.P. Kingma, J. Ba, Adam: A method for stochastic optimization, 2014, arXiv preprint arXiv:1412.6980.
[42] M.C. Cieslak, A.M. Castelfranco, V. Roncalli, P.H. Lenz, D.K. Hartline, T-distributed stochastic neighbor embedding (t-SNE): A tool for eco-physiological transcriptomic analysis, Mar. Genom. 51 (2020) 100723.
[43] T. Anwar, A machine learning approach for recognizing intellectual development disorder using eeg, in: 2020 International Conference on Biomedical Innovations and Applications, BIA, IEEE, 2020, pp. 9–12.
[44] J. Breitenbach, D. Raab, E. Fezer, D. Sauter, H. Baumgartl, R. Buettner, Automatic diagnosis of intellectual and developmental disorder using machine learning based on resting-state EEG recordings, in: 2021 17th International Conference on Wireless and Mobile Computing, Networking and Communications (WiMob), IEEE, 2021, pp. 7–12.
[45] K. Oda, N. Norouzi, EEG data analysis for intellectual developmental disorder, in: 2021 IEEE International Conference on Bioinformatics and Biomedicine, BIBM, IEEE, 2021, pp. 3662–3666.
[46] A. Topic, M. Russo, Emotion recognition based on EEG feature maps through deep learning network, Eng. Sci. Technol. Int. J. 24 (6) (2021) 1442–1454.
[47] T. Song, W. Zheng, P. Song, Z. Cui, EEG emotion recognition using dynamical graph convolutional neural networks, IEEE Trans. Affect. Comput. 11 (3) (2018) 532–541.
[48] Y. Yang, Q.J. Wu, W.-L. Zheng, B.-L. Lu, EEG-based emotion recognition using hierarchical network with subnetwork nodes, IEEE Trans. Cogn. Dev. Syst. 10 (2) (2017) 408–419.
[49] A. Subasi, T. Tuncer, S. Dogan, D. Tanko, U. Sakoglu, EEG-based emotion recognition using tunable Q wavelet transform and rotation forest ensemble classifier, Biomed. Signal Process. Control 68 (2021) 102648.
[50] N. Pusarla, A. Singh, S. Tripathi, Normal inverse Gaussian features for EEG-based automatic emotion recognition, IEEE Trans. Instrum. Meas. 71 (2022) 1–11.
[51] P.-f. Ke, D.-s. Xiong, J.-h. Li, Z.-l. Pan, J. Zhou, S.-j. Li, J. Song, X.-y. Chen, G.-x. Li, J. Chen, et al., An integrated machine learning framework for a discriminative analysis of schizophrenia using multi-biological data, Sci. Rep. 11 (1) (2021) 1–11.